JOURNAL OF PROPULSION AND POWER
Vol. 11, No. 1, January–February 1995

Spatial Instability of a Viscous Liquid Sheet

E. A. Ibrahim*
Tuskegee University, Tuskegee, Alabama 36088

The spatial instability theory is used to study the evolution of symmetrical and antisymmetrical disturbances of a moving viscous liquid sheet in an inviscid gas medium. The similarities and dissimilarities between spatial and temporal instabilities are delineated. Effects of properties such as viscosity, density, and surface tension on instability are examined. It is found that liquid viscosity always reduces the growth rate and dominant wave number for symmetrical disturbances. For antisymmetrical disturbances, liquid viscosity reduces the growth rate and dominant wave number at large Weber number, whereas liquid viscosity enhances instability at low Weber number. An increase in the gas-to-liquid density ratio always raises the growth rate of symmetrical disturbances. The growth rate of antisymmetrical disturbances initially increases with the density ratio, and then decreases when the density ratio exceeds Weber number. Surface tension always opposes the development of instability. Symmetrical disturbances control the instability for small Weber number, whereas antisymmetrical disturbances dominate for large Weber number. The dominant wave numbers associated with symmetrical disturbances are always greater than those of antisymmetrical disturbances.

Introduction

ATOMIZATION is a process whereby a volume of liquid is converted into a multiplicity of small drops. One of the most important applications of atomization is liquid fuel injection in internal combustion engines, gas turbines, and liquid-propellant rocket engines. In this case, the principal aim of the atomization process is to produce a high ratio of surface-to-mass in the liquid phase, which results in very high evaporation rates that contribute to raising the combustion efficiency and reducing environmental pollution.

In internal combustion engines, the liquid fuel is injected from an orifice in the form of a circular jet. The mechanism of breakup of circular liquid jets has been extensively studied.[1–5] Gas burners used in gas-turbine combustors employ swirl nozzles that cause the liquid fuel to be issued as a thin hollow-cone sheet. Most of the important features of sheet breakup processes in hollow-cone sprays may be reasonably understood by studying the stability of a moving thin liquid sheet of constant thickness.[6,7]

Despite its practical significance, there has been little theoretical investigation of the breakup of a liquid sheet. The basic study by Squire[6] treats the instability of an inviscid liquid sheet. Hagerty and Shea[8] conducted an experimental and theoretical study on a flat sheet of liquid produced by a slender orifice that was subjected to waves of different frequency. They concluded that only two types of waves are possible at any given frequency. Either the two surfaces of the sheet are in phase to produce antisymmetrical (sinusoidal) waves, or they oscillate out of phase to produce symmetrical (dilational) waves. Their results show that the principal sources of sheet instability are the aerodynamic forces arising from the interaction of the sheet with the surrounding gas medium. Taylor[7] analyzed the growth of wind-induced interface waves under the assumption of potential flow in the liquid and the surrounding gas with a discontinuity in velocity at the interface. Dombrowski and Johns[9] extended the analysis by including the effect of liquid viscosity and sheet thickness attenuation. However, Dombrowski and Johns'[9] results are only valid for large gas Weber number (ratio of the aerodynamic forces in the gas to the capillary forces in the liquid) owing to approximations made in their analysis.[10] Clark and Dombrowski[11] have applied a second-order theory to calculate the breakup lengths of attenuating sheets for the case where the wavelengths are relatively long compared with the sheet thickness. The large-amplitude theory of Crapper et al.[12] is restricted to a steady-state situation that the instability waves never really reach. Rangel and Sirignano[13,14] studied the effect of surface tension and density ratio on the nonlinear temporal growth of Kelvin-Helmholtz instability waves using the vortex-sheet discretization technique. Rangel and Hess[15] used the same technique to investigate the nonlinear spatial instability of a liquid sheet. However, this technique is only applicable to inviscid flow. Li and Tankin[10] presented a study of the temporal instability of a viscous liquid sheet of constant thickness that is valid at any Weber number. Li and Tankin[10] concluded that antisymmetrical perturbations control the instability process for large Weber numbers, whereas the symmetrical perturbations dominate for small Weber numbers. The absolute and convective instability of a viscous liquid sheet has been investigated by Lin et al.[16]

Crapper et al.[17] advanced experimental evidence that the growth of instability waves on liquid sheets takes place spatially, not temporally. It is now well recognized that both temporal and spatial growth need consideration in general.[18–20] The author is only aware of one attempt to investigate the spatial instability of a viscous liquid sheet, namely that of Chuech.[21] Chuech revised the temporal analysis of Dombrowski and Johns[9] to study the spatial instability of a viscous liquid sheet. However, Chuech's analysis is based on the same assumptions introduced by Dombrowski and Johns that lends his results to also be valid only for large Weber numbers. The present work is motivated by the need to develop a fundamental understanding of the spatial instability of liquid sheets that is at least at the same level of our understanding of temporal instability. The basic features of the spatial instability as well as the differences and similarities between spatial and temporal instability of a liquid sheet are investigated.

Problem Formulation

Consider a viscous liquid sheet of thickness $2a$ that is issued from a nozzle at a velocity U into a quiescent inviscid gas medium as shown in Fig. 1. The gas viscosity is neglected following Taylor's[2] treatment of a related problem. This ne-

Received Oct. 9, 1993; presented as Paper 94-0562 at the AIAA 32nd Aerospace Sciences Meeting, Reno, NV, Jan. 10–13, 1994; revision received April 30, 1994; accepted for publication May 10, 1994.

*Assistant Professor, Mechanical Engineering Department. Member AIAA.

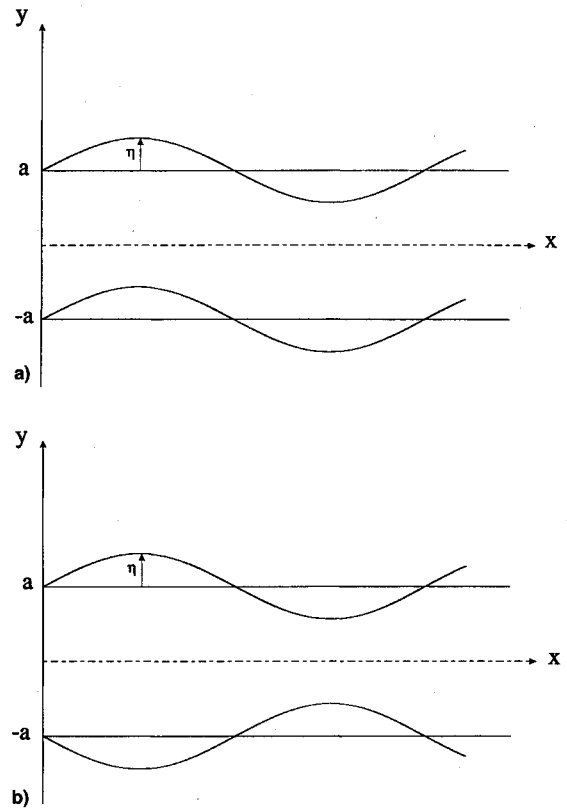

Fig. 1 a) Antisymmetrical and b) symmetrical disturbances.

glect of gas viscosity is based on the observation that the gas viscosity is weakly stabilizing, as has been demonstrated by Tomotika[22] and Lin and Ibrahim.[5] U is small compared to the velocity of sound, thus the assumption of incompressibility for both fluids is valid. Assume u, v are the liquid velocity components in the x, y directions, respectively, resulting from a disturbance, and p the pressure due to the disturbance. The x axis is parallel to the direction of U, and the y axis is normal to the undisturbed sheet surface with its origin at the midplane of the sheet. The equations of mass and momentum conservation that govern the liquid motion are linearized by neglecting all nonlinear terms in disturbance quantities, and may be written, respectively, as

$$\frac{\partial u}{\partial x} + \frac{\partial v}{\partial y} = 0 \tag{1}$$

$$\frac{\partial u}{\partial t} + U\frac{\partial u}{\partial x} = -\frac{1}{\rho_l}\frac{\partial p}{\partial x} + \nu_l\left(\frac{\partial^2 u}{\partial x^2} + \frac{\partial^2 u}{\partial y^2}\right) \tag{2}$$

$$\frac{\partial v}{\partial t} + U\frac{\partial v}{\partial x} = -\frac{1}{\rho_l}\frac{\partial p}{\partial y} + \nu_l\left(\frac{\partial^2 v}{\partial x^2} + \frac{\partial^2 v}{\partial y^2}\right) \tag{3}$$

where t is the time, and ρ_l and ν_l are the liquid density and kinematic viscosity, respectively. The boundary conditions that Eqs. (1–3) are subjected to depend on whether the sheet disturbance is antisymmetrical or symmetrical as can be seen from Fig. 1. For antisymmetrical disturbances, the displacements of corresponding points on the two interfaces are equal in magnitude and in the same direction. For symmetrical disturbances the displacements are equal but occur in opposite directions. Therefore, for antisymmetrical disturbances the two interfaces are regarded to have the following form:

$$y = a + \eta, \qquad y = -a + \eta \tag{4}$$

For symmetrical disturbances the two interfaces have the form

$$y = a + \eta, \qquad y = -a - \eta \tag{5}$$

where η is the interface displacement at time t and distance x along the interface. The boundary conditions for Eqs. (1–3) at the two interfaces, which may be taken as $y \approx \pm a$, are that the velocity v at the interface is equal to the total derivative of the interface displacement. Since the surrounding gas medium is assumed to be inviscid, the tangential stresses should vanish at the interfaces. The normal stresses across the interface should be balanced. For antisymmetrical disturbances, these boundary conditions may be written, respectively, as

$$v = \frac{\partial \eta}{\partial t} + U\frac{\partial \eta}{\partial x} \quad \text{at} \quad y \approx \pm a \tag{6}$$

$$\mu_l\left(\frac{\partial u}{\partial y} + \frac{\partial v}{\partial x}\right) = 0 \quad \text{at} \quad y \approx \pm a \tag{7}$$

$$-p + 2\mu_l\frac{\partial v}{\partial y} = -p_g + p_\sigma \quad \text{at} \quad y \approx \pm a \tag{8}$$

where μ_l is the liquid dynamic viscosity, p_g is the gas pressure, and p_σ is the pressure due to surface tension. For symmetrical disturbances, the only boundary condition that changes form is the kinematic condition at $y \approx -a$, which becomes

$$v = -\left(\frac{\partial \eta}{\partial t} + U\frac{\partial \eta}{\partial x}\right) \quad \text{at} \quad y \approx -a \tag{9}$$

in accordance with the form of Eq. (5). The stream function of the liquid motion ψ is given by

$$u = \frac{\partial \psi}{\partial y}, \qquad v = -\frac{\partial \psi}{\partial x} \tag{10}$$

The equation of mass conservation Eq. (1) is readily satisfied by substitution from Eq. (10). The stream function may be represented by its Fourier series components and we may focus our attention on one of these components, which is written as

$$\psi = \Psi(y)\exp(ikx + \omega t) \tag{11}$$

For spatial instability analysis, k is a complex variable $k = k_r + ik_i$, and ω is an imaginary variable $\omega = i\omega_i$. The real part of k, k_r represents the wave number (2π divided by the wavelength) of the disturbance, and the imaginary part k_i represents the rate of growth or decay of the disturbance depending on whether k_i is negative or positive, respectively. The imaginary variable ω_i is 2π times the disturbance frequency, $-\omega_i/k_r$ is the wave propagation velocity, and $-\partial\omega_i/\partial k_r$ is the group velocity of the disturbances. Similarly, the interfacial displacement η may be expressed as

$$\eta = \eta_0 \exp(ikx + \omega t) \tag{12}$$

where η_0 is the amplitude of the initial disturbance. Eliminating the pressure from Eqs. (2) and (3) by cross differentiation and then substituting from Eq. (11) we get

$$\frac{d^4\Psi(y)}{dy^4} - (s^2 + k^2)\frac{d^2\Psi(y)}{dy^2} + k^2s^2\Psi(y) = 0 \tag{13}$$

where

$$s^2 = [k^2 + (\omega/\nu_l) + (ikU/\nu_l)] \tag{14}$$

The general solution of Eq. (13) is given by

$$\Psi(y) = [(C_1e^{ky} + C_2e^{-ky}) + (C_3e^{sy} + C_4e^{-sy})] \tag{15}$$

where C_1, C_2, C_3, and C_4 are constants of integration that are determined from the boundary conditions (6) and (7) in accordance with Eqs. (10–12), (14), and (15) to be

$$C_1 = C_2 = i\eta_0\nu_l[(k^2 + s^2)/2k \cosh(ka)] \quad (16)$$

$$C_3 = C_4 = -i\eta_0\nu_l[k/\cosh(sa)] \quad (17)$$

Substituting from Eqs. (15–17) into Eq. (11) we get the stream function of liquid motion as

$$\psi = 2[C_1 \cosh(ky) + C_3 \cosh(sy)]\exp(ikx + \omega t) \quad (18)$$

where C_1 and C_3 are given by Eqs. (16) and (17), respectively.

The liquid pressure due to disturbance p may be represented by

$$p = P(y)\exp(ikx + \omega t) \quad (19)$$

in accordance with the form of Eq. (11). The pressure p may now be determined from either Eq. (2) or (3) by substitution from Eqs. (10), (11), (16–19) to yield

$$p = 2i\rho_l(\omega + ikU)C_1 \sinh(ky)\exp(ikx + \omega t) \quad (20)$$

In the present analysis, the effect of the surrounding gas medium on the instability of liquid sheet is through the normal stress in boundary condition (8). The gas medium is assumed to be inviscid and quiescent before the disturbances set in. The mass conservation equation is then

$$\frac{\partial u_g}{\partial x} + \frac{\partial v_g}{\partial y} = 0 \quad (21)$$

where subscript g denotes quantities for the gas medium.

The gas velocity can be expressed in terms of a velocity potential, ϕ_g, such that

$$u_g = \frac{\partial \phi_g}{\partial x}, \qquad v_g = \frac{\partial \phi_g}{\partial y} \quad (22)$$

Furthermore, the velocity potential for the inviscid gas motion is assumed to be

$$\phi_g = \Phi_g(y)\exp(ikx + \omega t) \quad (23)$$

The boundary conditions for the inviscid gas require that across the liquid-gas interface the y-component velocity be continuous, and far away from the liquid surface the disturbances decay to zero. Hence, the boundary conditions for the upper half-plane are

$$v_g = \frac{\partial \phi_g}{\partial y} = \frac{\partial \eta}{\partial t} \quad \text{at} \quad y \approx a \quad (24)$$

$$v_g = \frac{\partial \phi_g}{\partial y} = 0 \quad \text{at} \quad y \to \infty \quad (25)$$

Substituting from Eq. (22) into Eq. (21) and the boundary conditions (24) and (25) yields

$$\phi_g = -(\omega/k)\exp[k(a - y)]\eta_0 \exp(ikx + \omega t) \quad (26)$$

The gas pressure may be calculated from the integrated momentum equation for the gas medium

$$p_g = -\rho_g \frac{\partial \phi_g}{\partial t} \quad (27)$$

which upon substitution from Eq. (26) gives

$$p_g = \rho_g(\omega^2/k)\exp[k(a - y)]\eta_0 \exp(ikx + \omega t) \quad (28)$$

The pressure induced by surface tension is, to the first order in η

$$p_\sigma = \frac{\sigma}{R} \approx \sigma \frac{\partial^2 \eta}{\partial x^2} = -\sigma k^2 \eta_0 \exp(ikx + \omega t) \quad \text{at} \quad y \approx a \quad (29)$$

where σ is the surface tension, and R is the radius of curvature of the liquid-gas interfaces. Substitution from Eqs. (10), (16–18), (20), (28), and (29) into the normal stress boundary condition (8) for $y = a$, leads to the following dispersion relation between k and ω:

$$[\rho_l(\omega + ikU) + 2\mu_l k^2][\nu_l(k^2 + s^2)]\tanh(ka) - 4\mu_l\nu_l k^3 s \tanh(sa) + \rho_g\omega^2 + \sigma k^3 = 0 \quad (30)$$

The derivation process of the dispersion relation for symmetrical disturbances is very similar to that for antisymmetrical ones. The governing equations are exactly the same, but the kinematic boundary condition for the liquid phase at $y \approx -a$ is different, as pointed out earlier in Eq. (9). The dispersion relation for symmetrical disturbances is similar to Eq. (30) except that $\tanh(ka)$ and $\tanh(sa)$ are replaced by $\coth(ka)$ and $\coth(sa)$, respectively:

$$[\rho_l(\omega + ikU) + 2\mu_l k^2][\nu_l(k^2 + s^2)]\coth(ka) - 4\mu_l\nu_l k^3 s \coth(sa) + \rho_g\omega^2 + \sigma k^3 = 0 \quad (31)$$

Equations (30) and (31) are similar to Eqs. (37) and (38) of Li and Tankin,[10] except that ω is purely imaginary and k is complex for the present spatial analysis, although ω is complex and k is real in Li and Tankin's[10] temporal analysis. However, the derivation procedure of Eqs. (30) and (31) in the present investigation is quite different from that of Li and Tankin. In their formulation, Li and Tankin determined the pressure in the viscous liquid from the relations applicable to inviscid liquid because the presence of viscosity affects the wave frequency, but not the pressure within the liquid as pointed out by Levich.[23] Although their approach is correct, it is unnecessary and it leads to a more complicated derivation. The present formulation allows for direct evaluation of the viscous liquid pressure via the stream function of the liquid motion.

Results and Discussion

To facilitate the analysis, Eqs. (30) and (31) are respectively expressed in dimensionless form as follows:

$$\frac{m_1^2}{Re^2}\tanh(K) - \frac{4m^{1/2}}{Re^2}K^3 \tanh(m^{1/2}) - \rho\Omega_i^2 + \frac{\rho}{We_g}K^3 = 0 \quad (32)$$

$$\frac{m_1^2}{Re^2}\coth(K) - \frac{4m^{1/2}}{Re^2}K^3 \coth(m^{1/2}) - \rho\Omega_i^2 + \frac{\rho}{We_g}K^3 = 0 \quad (33)$$

where $\Omega_i = \omega_i(a/U)$, $K = K_r + iK_i = (k_r + ik_i)a = ka$, $\rho = (\rho_g/\rho_l)$, $m = [K^2 + iRe(\Omega_i + K)]$, $m_1 = m + K^2$. Re is the liquid Reynolds number $Re = Ua/\nu_l$, and We_g is the gas Weber number $We_g = \rho_g U^2 a/\sigma$. For an inviscid liquid sheet, $Re \to \infty$, and Eqs. (32) and (33) readily reduce to

$$-(\Omega_i + K)^2 \tanh(K) - \rho\Omega_i^2 + (\rho/We_g)K^3 = 0 \quad (34)$$

$$-(\Omega_i + K)^2 \coth(K) - \rho\Omega_i^2 + (\rho/We_g)/K^3 = 0 \quad (35)$$

respectively. Equations (32–35) are solved numerically using Muller's[24] method to yield values of K as a function of Ω_i for different values of the dimensionless parameters ρ, Re, and We_g. The IMSL Fortran subroutine ZANLY uses Muller's method with deflation to find a real or complex root of an arbitrary complex function given an initial guess of the root (i.e., $K = K_r + iK_i$). In providing the guessed root it is helpful to realize that $k_r \approx -\omega_i$ in accordance with Gaster's[25] theorem.

Figure 2 shows a comparison between the predictions of the spatial and temporal growth rates of antisymmetrical disturbances for $\rho = 0.1$, $We_g = 4.0$, and $Re = \infty$, 63.25. A similar comparison for symmetrical disturbances is shown in Fig. 3. Equations (39–42) of Li and Tankin[10] are used to obtain the temporal growth rate results shown in Figs. 2 and 3. However, the temporal growth rate of Li and Tankin was divided by the square root of the liquid Weber number $We_l = \rho_l U^2 a/\sigma = We_g/\rho$, to be made dimensionless in the same manner as the present spatial growth rate.

It can be seen from Figs. 2 and 3 that, for an inviscid liquid sheet, the spatial instability growth rate and limiting wave number are always larger than that of temporal instability. The effect of viscosity in the liquid is to cause the growth rates of both spatial and temporal instability to approach each other, especially near the higher values of wave number. The limiting wave numbers of both spatial and temporal instability are identical and equal to We_g for viscous liquid sheets. Note that the limiting wave number can be obtained by setting $K_i = 0$ in Eq. (32) or (33) for antisymmetrical and symmetrical disturbances, respectively. Both Eq. (32) or (33) give the limiting wave number as $K_r = We_g$.

Li and Tankin have shown that the limiting wave number of temporal instability is also equal to We_g for both antisymmetrical and symmetrical disturbances. For inviscid liquid sheets undergoing spatial instability the limiting wave number is a function of ρ, We_g, and Ω_i, as can be seen from Eqs. (34) and (35). It is not possible to eliminate Ω_i from Eqs. (34) or (35) by separation of each of the equations into real and imaginary components as has been done in the temporal instability analysis of Li and Tankin.

The effect of liquid viscosity on the spatial instability of liquid sheets is investigated further in Figs. 4 and 5 for antisymmetrical and symmetrical disturbances, respectively, for $\rho = 0.1$, $We_g = 4.0$, and $Re = \infty$, 63.25, 1.25. It is seen from Figs. 4 and 5 that liquid viscosity, affected through Reynolds number, reduces both the disturbance growth rate and shifts the dominant wave of the disturbances to a longer wavelength. The limiting wave number of inviscid liquid sheets is less than that of viscous liquid sheets, which is fixed at the value $K_r = We_g$ as discussed earlier. In their photographical study of the disintegration of liquid sheets, Dombrowski and Fraser[26] concluded that increasing liquid viscosity yields a more stable sheet in agreement with the present results. This damping effect of viscosity is due to its role as a mechanism of energy dissipation.

Squire[6] reported that when the gas Weber number falls below a critical value $We_g = \rho$, there will be no instability arising from the antisymmetrical long-wave disturbances of an inviscid liquid sheet. For a viscous liquid sheet subjected

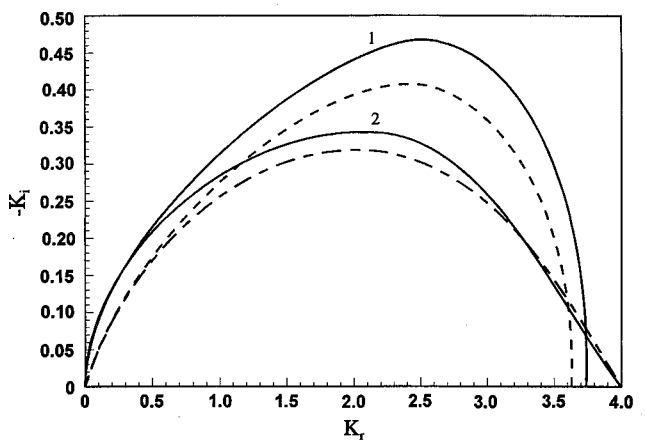

Fig. 2 Comparison of spatial and temporal instability of antisymmetrical disturbances. $\rho = 0.1$ and $We_g = 4.0$. Curve 1, spatial, $Re = \infty$, curve 2, spatial, $Re = 63.25$, dashed curve, temporal, $Re = \infty$, centerlined curve, temporal, $Re = 63.25$.

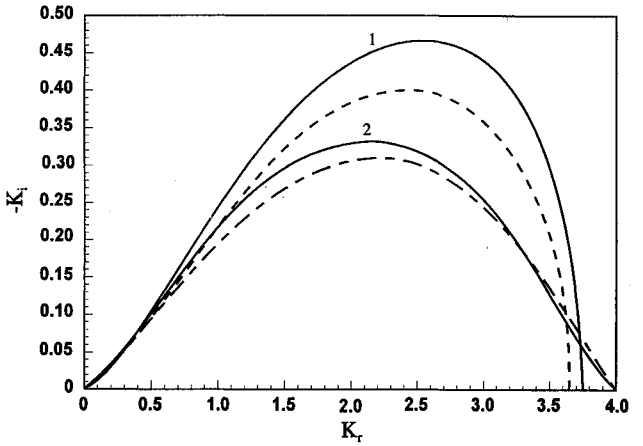

Fig. 3 Comparison of spatial and temporal instability of symmetrical disturbances. $\rho = 0.1$ and $We_g = 4.0$. Curve 1, spatial, $Re = \infty$, curve 2, spatial, $Re = 63.25$, dashed curve, temporal, $Re = \infty$, centerlined curve, temporal, $Re = 63.25$.

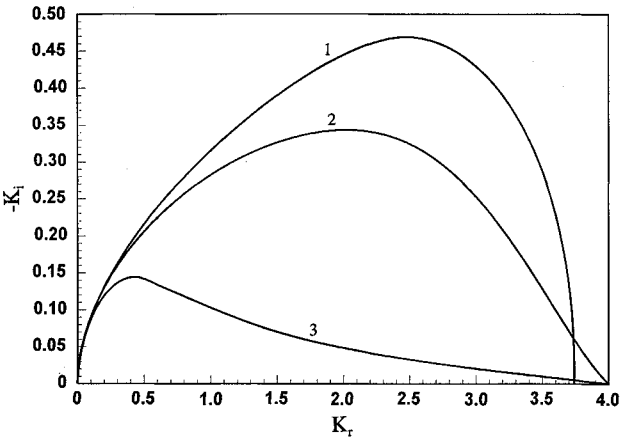

Fig. 4 Effect of liquid viscosity on antisymmetrical disturbances. $\rho = 0.1$ and $We_g = 4.0$. Curve 1, $Re = \infty$, curve 2, $Re = 63.25$, curve 3, $Re = 1.25$.

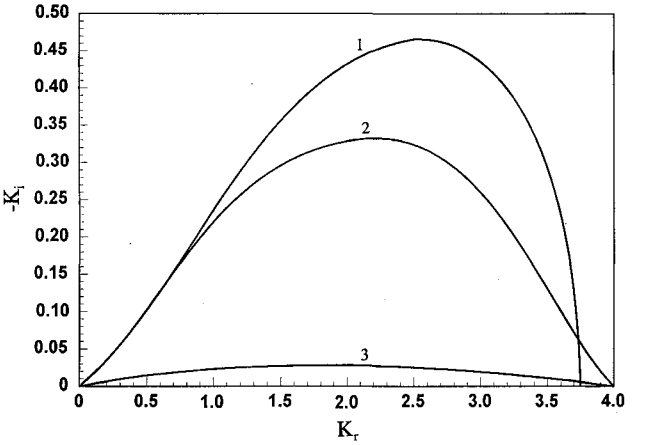

Fig. 5 Effect of liquid viscosity on symmetrical disturbances. $\rho = 0.1$ and $We_g = 4.0$. Curve 1, $Re = \infty$, curve 2, $Re = 63.25$, curve 3, $Re = 1.25$.

to antisymmetrical disturbances, Li and Tankin observed that if the gas Weber number is slightly larger than its critical value, there exist two local maxima for the growth rate of the disturbance. These two different modes of instability were termed aerodynamic and viscosity-enhanced by Li and Tankin. At low gas Weber number $We_g \approx \rho$, liquid viscosity has little effect on the aerodynamic mode of instability, and growth rates of inviscid and viscous liquid sheets are essentially the same. At high gas Weber number, aerodynamic instability is hindered by liquid viscosity as has been discussed with regard to Figs. 4 and 5. The viscosity-enhanced mode is characterized by the increase of the growth rate of the disturbances with viscosity. At gas Weber numbers less than the critical value $We_g = \rho$, aerodynamic instability disappears completely, and only viscosity-enhanced instability will exist.

To explore the existence of such double modes in the spatial instability arising from antisymmetrical disturbances, computations have been carried out for $\rho = 0.1$, $We_g = 0.13$, and $Re = 0.2, 0.25$, using Eq. (32). The results are depicted in Figs. 6 and 7, which show the aerodynamic and viscosity-enhanced instabilities, respectively. Although these two modes of instabilities occur simultaneously, they are plotted separately in Figs. 6 and 7 because the magnitudes of the growth rate of aerodynamic instability are much larger than that of viscosity-enhanced. However, Li and Tankin[10] demonstrated that the viscosity-enhanced mode dominated the instability process when the gas Weber number is slightly above the critical value $We_g = \rho$, specifically at $We_g = 0.1025$ and $\rho = 0.1$. As Weber number is increased aerodynamic instability continues to grow while the viscosity-enhanced instability is greatly diminished.

For symmetrical disturbances, the growth rate curves are always similar to those shown in Fig. 5, whether the gas Weber number is small or large. Aerodynamic instability always prevails, and viscosity-enhanced instability has no local maximum growth rate. There is no critical value of Weber number for symmetrical disturbances.

Figures 8 and 9 illustrate the effect of gas-to-liquid density ratio on the growth rates of spatial instability due to antisymmetrical and symmetrical disturbances, respectively. The data in Figs. 8 and 9 correspond to $We_g = 0.9$ and $Re = 1.0$. The density ratio varies as $\rho = 2.0, 1.0, 0.10$, and 0.01 for antisymmetrical disturbances, and $\rho = 1.0, 0.1$, and 0.05 for symmetrical disturbances. It is seen in Fig. 8 that an increase in the gas-to-liquid density ratio increases the growth rate and dominant wave number of the antisymmetrical disturbances as long as the density ratio is less than the gas Weber number. Once the density ratio becomes greater than the gas Weber number the disturbance growth rate is reduced with further increase of the density ratio. A density ratio higher than the gas Weber number shifts the mechanism of instability from aerodynamic to viscosity-enhanced since the gas Weber number becomes less than its critical value $We_g = \rho$. Viscosity-enhanced instability is typically associated with lower growth rates, as has been discussed earlier. For symmetrical disturbances, Fig. 9 shows that the density ratio always enhances the instability, as expected, since no critical gas Weber number exists. The present results are in general agreement with Dombrowski and Hooper's[27] experimental observations in their study of the effect of ambient density on the stability and disintegration of flat sheets.

The effect of surface tension, through the gas Weber number, on the spatial instability by antisymmetrical and symmetrical disturbances is investigated in Figs. 10 and 11, re-

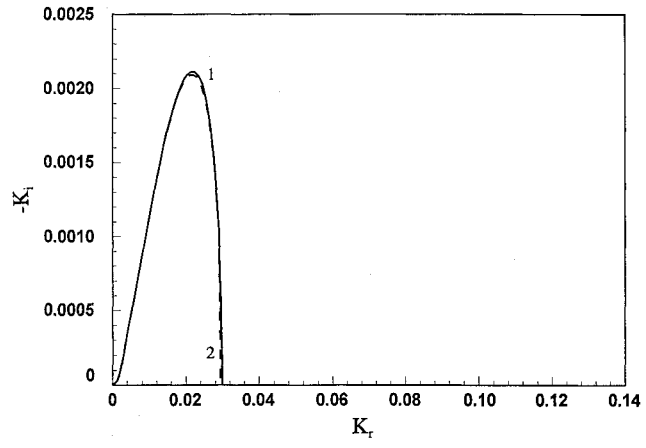

Fig. 6 Aerodynamic instability of antisymmetrical disturbances. $\rho = 0.1$ and $We_g = 0.13$. Curve 1, $Re = 0.25$, curve 2, $Re = 0.2$.

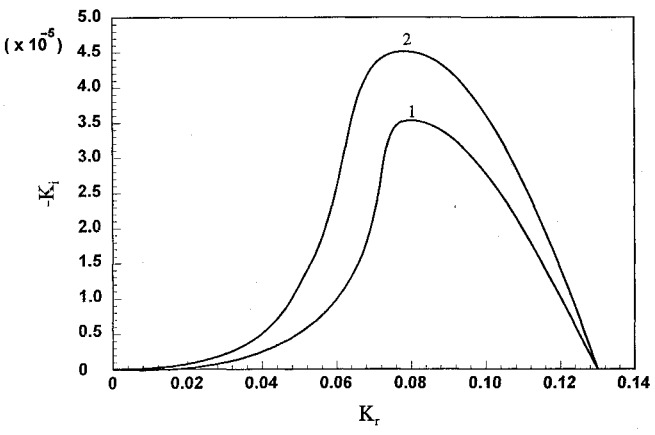

Fig. 7 Viscosity-enhanced instability of antisymmetrical disturbances. $\rho = 0.1$ and $We_g = 0.13$. Curve 1, $Re = 0.25$, curve 2, $Re = 0.2$.

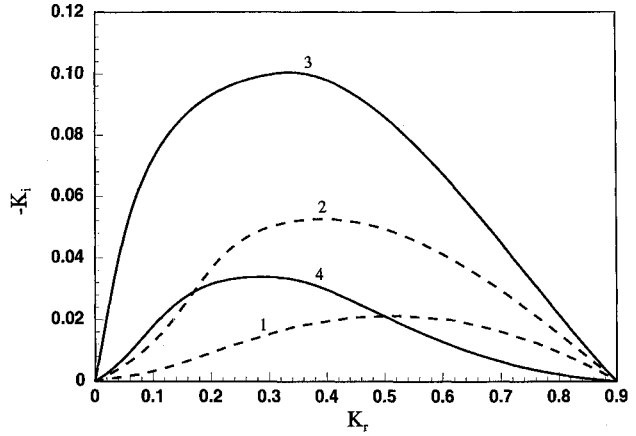

Fig. 8 Effect of density ratio on instability of antisymmetrical disturbances. $We_g = 0.9$ and $Re = 1.0$. Curve 1, $\rho = 2.0$, curve 2, $\rho = 1.0$, curve 3, $\rho = 0.1$, curve 4, $\rho = 0.01$.

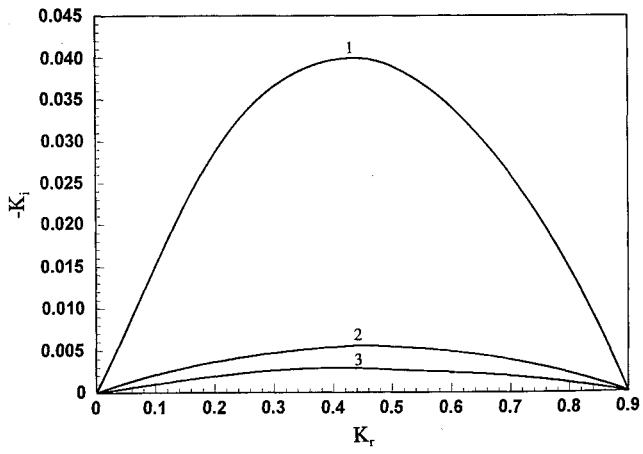

Fig. 9 Effect of density ratio on instability of symmetrical disturbances. $We_g = 0.9$ and $Re = 1.0$. Curve 1, $\rho = 1.0$, curve 2, $\rho = 0.1$, curve 3, $\rho = 0.05$.

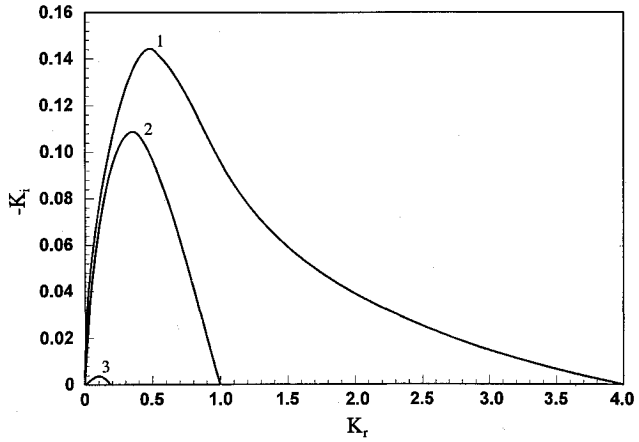

Fig. 10 Effect of gas Weber number on instability of antisymmetrical disturbances. $\rho = 0.1$ and $Re = 1.25$. Curve 1, $We_g = 4.0$, curve 2, $We_g = 1.0$, curve 3, $We_g = 0.16$.

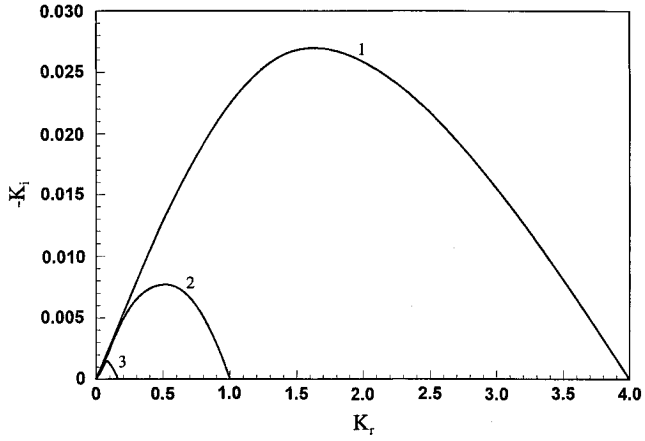

Fig. 11 Effect of gas Weber number on instability of symmetrical disturbances. $\rho = 0.1$ and $Re = 1.25$. Curve 1, $We_g = 4.0$, curve 2, $We_g = 1.0$, curve 3, $We_g = 0.16$.

spectively, for $\rho = 0.1$, $Re = 1.25$ and $We_g = 0.16$, 1.0, 4.0. The trend in Figures 10 and 11 is that decreasing the gas Weber number reduces the growth rate and the instability limit and shifts the dominant wave number to a longer wavelength. This means that surface tension always acts to stabilize the liquid sheet, i.e., to damp out the disturbances. This monotonic effect of surface tension on instability is evident from Eqs. (34) and (35). Dombrowski and Fraser[26] have observed experimentally that an increase in surface tension produced a reduction in the spray angle and increased sheet breakup length.

Figure 12 shows the maximum growth rate as a function of gas Weber number for the spatial instability of a viscous liquid sheet at $\rho = 0.1$ and $Re = 1.25$. Figure 12a indicates that at small gas Weber number, symmetrical disturbances have a larger growth rate than antisymmetrical ones; they dominate the instability process. As the gas Weber number increases, the growth rate for both types of disturbances increases. However, that of antisymmetrical disturbances increases much faster and, above a certain gas Weber number, antisymmetrical disturbances become predominant (Fig. 12a), and maintain this dominance from there on (Fig. 12b). This is especially true at lower values of density ratios. Li and Tankin[10] have shown that for an inviscid liquid sheet the maximum growth rate for both types of disturbances approach each other when the gas Weber number becomes very large. At low gas Weber number, symmetrical disturbances of an inviscid liquid sheet prevail over antisymmetrical ones in a fashion similar to that shown in Fig. 12a. Below the critical value $We_g = \rho$, the instability of an inviscid sheet is possible only via symmetrical

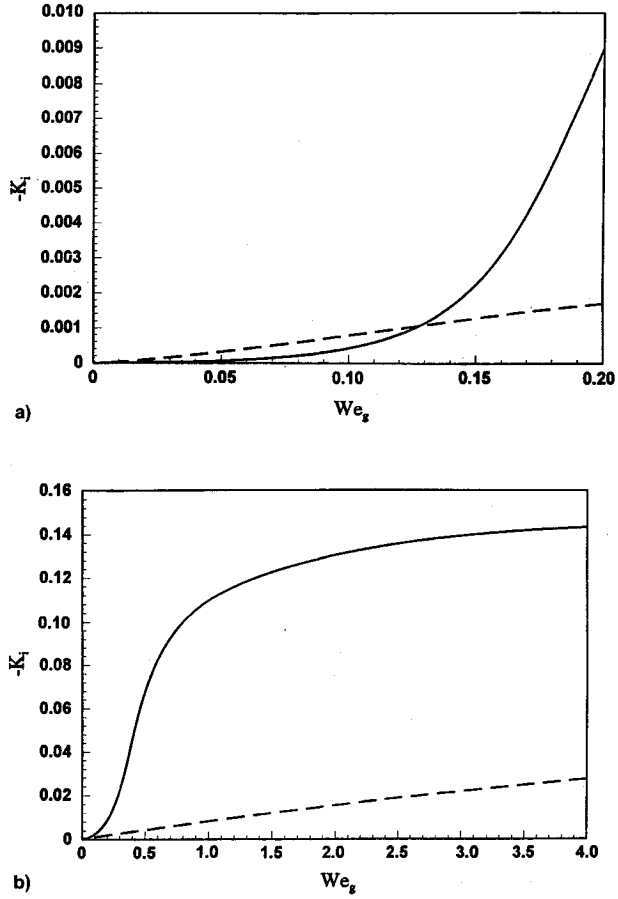

Fig. 12 Maximum growth rate for a viscous liquid sheet. $\rho = 0.1$ and $Re = 1.25$. Solid curve, antisymmetrical disturbances, dashed curve, symmetrical disturbances.

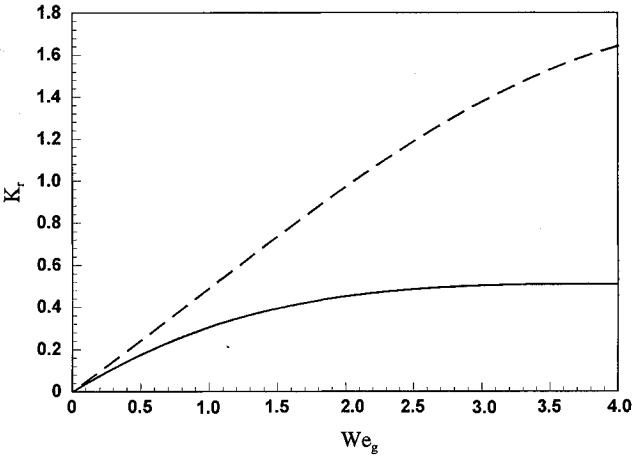

Fig. 13 Dominant wave number for a viscous liquid sheet. $\rho = 0.1$ and $Re = 1.25$. Solid curve, antisymmetrical disturbances, dashed curve, symmetrical disturbances.

disturbances. Note that in Fig. 12a the maximum growth rate for antisymmetrical disturbances correspond to viscosity-enhanced instability when the gas Weber number is under the critical value $We_g = \rho = 0.1$. Above the critical value the maximum growth rate for antisymmetrical disturbances corresponds to aerodynamic instability.

Figure 13 shows the dominant wave number that corresponds to maximum growth rate for antisymmetrical and symmetrical disturbances for $\rho = 0.1$ and $Re = 1.25$. The dominant wave number for symmetrical disturbances is always greater than the corresponding value for antisymmetrical ones. Li and Tankin demonstrated that for an inviscid liquid sheet,

the dominant wave number of symmetrical disturbances is greater than that of antisymmetrical disturbances, except for very large gas Weber number where both types of disturbances reach asymptotically the same dominant wave number. However, for a viscous liquid sheet, the dominant wave number of symmetrical disturbances continue to increase faster than that of antisymmetrical disturbances as can be seen from Fig. 13.

Conclusions

The spatial instability of a viscous liquid sheet in an inviscid gas medium with respect to symmetrical and antisymmetrical disturbances is investigated. It is found that the growth rate and instability limit of spatial instability are always larger than those associated with temporal instability. The effects of liquid viscosity, surface tension, and gas-to-liquid density ratio on instability are reported. For a viscous liquid sheet two modes of instability coexist, namely, aerodynamic and viscosity-enhanced in contrast to inviscid liquid sheets for which the only mode of instability is aerodynamic. For symmetrical disturbances, aerodynamic instability prevails and liquid viscosity always reduces the growth rate and the dominant wave number. For antisymmetrical disturbances, the relative magnitude of the gas Weber number and gas-to-liquid density ratio dictates which instability mode predominates. If the gas Weber number is large compared to the gas-to-liquid density ratio, the instability is due to aerodynamic effects. The growth rate and dominant wave number of antisymmetrical disturbances are reduced as the liquid viscosity is increased. At gas Weber numbers that are smaller than the gas-to-liquid density ratio, viscosity-enhanced instability is the only possible mode of instability, and liquid viscosity promotes instability. Increasing the gas-to-liquid density ratio raises the growth rate of symmetrical and antisymmetrical disturbances. However, the gas-to-liquid density ratio reduces the growth rate of antisymmetrical disturbances if the gas Weber number falls below a critical value $We_g = \rho$, since the instability mechanism is then changed to that of viscosity-enhanced. The surface tension, effected through Weber number, always acts as a stabilizing agent. It is also found that symmetrical disturbances control the instability process for small gas Weber number, while antisymmetrical disturbances dominate for large Weber number. The dominant wave number of symmetrical disturbances is always greater than that of antisymmetrical disturbances. It should be noted that although the salient features of sheet instability are predictable through linear stability analysis, the results are only valid for the initial stages of sheet instability when the disturbance amplitudes are infinitesimally small. A nonlinear theory is needed to accurately predict important atomization parameters such as breakup length, spray angle, and drop size.

Acknowledgment

This work has been supported by Grant F49620-92-J-0194 from the Air Force Office of Scientific Research, Bolling Air Force Base, Washington, DC.

References

[1]Rayleigh, L., *The Theory of Sound*, Dover, New York, 1945, p. 351.

[2]Taylor, G. I., "Generation of Ripples by Wind Blowing over Viscous Fluids," *The Scientific Papers of G. I. Taylor*, Vol. 3, No. 25, Cambridge Univ. Press, Cambridge, England, UK, 1963, pp. 244–254.

[3]Bogy, D. B., "Drop Formation in a Circular Liquid Jet," *Annual Review of Fluid Mechanics*, Vol. 11, 1979, pp. 207–228.

[4]Lin, S. P., and Lian, Z. W., "Mechanism of the Breakup of Liquid Jets," *AIAA Journal*, Vol. 28, No. 1, 1990, pp. 120–126.

[5]Lin, S. P., and Ibrahim, E. A., "Instability of a Viscous Liquid Jet Surrounded by a Viscous Gas in a Vertical Pipe," *Journal of Fluid Mechanics*, Vol. 218, Sept. 1990, pp. 641–658.

[6]Squire, H. B., "Investigation of the Instability of a Moving Fluid Film," *British Journal of Applied Physics*, Vol. 4, June 1953, pp. 167–169.

[7]Taylor, G. I., "The Dynamics of Thin Sheets of Fluid," *Proceedings of the Royal Society of London*, Vol. A253, Dec. 1959, pp. 289–321.

[8]Hagerty, W. W., and Shea, J. F., "A Study of the Instability of Plane Fluid Sheets," *Journal of Applied Mechanics*, Vol. 22, Dec. 1955, pp. 509–514.

[9]Dombrowski, N., and Johns, W. R., "The Aerodynamic Instability and Disintegration of Viscous Liquid Sheets," *Chemical Engineering Science*, Vol. 18, No. 3, 1963, pp. 203–214.

[10]Li, X., and Tankin, R. S., "On the Instability of a Two-Dimensional Viscous Liquid Sheet," *Journal of Fluid Mechanics*, Vol. 226, May 1991, pp. 425–443.

[11]Clark, C. J., and Dombrowski, N., "Aerodynamic Instability and Disintegration of Inviscid Liquid Sheets," *Proceedings of the Royal Society of London*, Vol. A329, No. 1579, 1972, pp. 467–478.

[12]Crapper, G. D., Dombrowski, N., and Pyott, G. A. D., "Large Amplitude Kelvin-Helmholtz Waves on Thin Liquid Sheets," *Proceedings of the Royal Society of London*, Vol. A342, No. 1629, 1975, pp. 209–224.

[13]Rangel, R. H., and Sirignano, W. A., "Nonlinear Growth of Kelvin-Helmholtz Instability: Effect of Surface Tension and Density Ratio," *Physics of Fluids*, Vol. 31, No. 7, 1988, pp. 1845–1855.

[14]Rangel, R. H., and Sirignano, W. A., "The Linear and Nonlinear Shear Instability of a Fluid Sheet," *Physics of Fluids A*, Vol. 3, No. 10, 1991, pp. 2392–2400.

[15]Rangel, R. H., and Hess, C., "Nonlinear Spatial Instability of a Fluid Sheet," AIAA Paper 90-0118, Jan. 1990.

[16]Lin, S. P., Lian, Z. W., and Creighton, B. J., "Absolute and Convective Instability of a Liquid Sheet," *Journal of Fluid Mechanics*, Vol. 220, Nov. 1990, pp. 673–689.

[17]Crapper, G. D., Dombrowski, N., Jepson, W. P., and Pyott, G. A. D., "A Note on the Growth of Kelvin-Helmholtz Waves on Thin Liquid Sheets," *Journal of Fluid Mechanics*, Vol. 57, Pt. 4, 1973, pp. 671, 672.

[18]Keller, J. B., Rubinow, S. I., and Tu, Y. O., "Spatial Instability of a Jet," *Physics of Fluids*, Vol. 16, Dec. 1972, pp. 2052–2055.

[19]Lin, S. P., and Kang, D. J., "Atomization of a Liquid Jet," *Physics of Fluids*, Vol. 30, No. 7, 1987, pp. 2000–2006.

[20]Huerre, P., and Monkewitz, P. A., "Local and Global Instabilities in Spatially Developing Flows," *Annual Review of Fluid Mechanics*, Vol. 22, 1990, pp. 473–537.

[21]Chuech, S. G., "A Comparative Study of Temporal and Spatial Instabilities of a Two-Dimensional Liquid Sheet," *Proceedings of the Winter Annual Meeting of the American Society of Mechanical Engineers*, HTD-Vol. 187, Dec. 1991, pp. 19–25.

[22]Tomotika, S., "On the Instability of a Cylindrical Thread of a Viscous Liquid Surrounded by Another Viscous Fluid," *Proceedings of the Royal Society*, Vol. 150, Series A, No. 870, 1935, pp. 322–337.

[23]Levich, V. G., *Physicochemical Hydrodynamics*, Prentice-Hall, Englewood Cliffs, NJ, 1962, p. 600.

[24]Muller, D. E., "A Method for Solving Algebraic Equations Using an Automatic Computer," *Mathematical Tables and Aids to Computation*, Vol. 10, No. 5, 1956, pp. 208–215.

[25]Gaster, M., "A Note on the Relation Between Temporally-Increasing and Spatially-Increasing Disturbances in Hydrodynamic Stability," *Journal of Fluid Mechanics*, Vol. 14, Pt. 2, Oct. 1962, pp. 222–224.

[26]Dombrowski, N., and Fraser, R. P., "A Photographic Investigation into the Disintegration of Liquid Sheets," *Philosophical Transactions of the Royal Society of London*, Vol. A247, Sept. 1954, pp. 101–130.

[27]Dombrowski, N., and Hooper, P. C., "The Effect of Ambient Density on Drop Formation in Sprays," *Chemical Engineering Science*, Vol. 17, April 1962, pp. 291–305.